PAPER

A novel magneto-rheological fluid dual-clutch design for two-speed transmission of electric vehicles

To cite this article: Huan Zhang *et al* 2021 *Smart Mater. Struct.* **30** 075035

IOP Publishing Smart Materials and Structures
Smart Mater. Struct. **30** (2021) 075035 (12pp) https://doi.org/10.1088/1361-665X/ac0674

A novel magneto-rheological fluid dual-clutch design for two-speed transmission of electric vehicles

Huan Zhang[1], Haiping Du[1], Shuaishuai Sun[2], Jin Zhao[1], Donghong Ning[1], Weihua Li[2] and Yafei Wang[3]

[1] School of Electrical, Computer and Telecommunications Engineering, University of Wollongong, Wollongong, NSW 2522, Australia
[2] School of Mechanical, Materials, Mechatronic and Biomedical Engineering, University of Wollongong, Wollongong, NSW 2522, Australia
[3] School of Mechanical and Power Engineering, Shanghai Jiao Tong University, Shanghai 200000, People's Republic of China

E-mail: hdu@uow.edu.au

Received 20 March 2021, revised 12 May 2021
Accepted for publication 27 May 2021
Published 17 June 2021

Abstract

The dual-clutch transmission (DCT) in electric vehicles can significantly decrease the torque interruption and improve the shifting comfort. The magneto-rheological fluid (MRF) is a kind of intelligent material commonly used for torque transmission devices with high control accuracy and fast response, e.g. MRF clutch. This paper proposes a novel MRF dual-clutch (MRFDC) design for the two-speed transmission of EVs combining the DCT and MRF clutch advantages. The MRFDC is composed of an internal clutch and an external clutch. The two clutches with the same input shaft and different output shaft can shift between two gears by controlling the input current through the coils in the two clutches. The relationship between the input current and the magnetic flux density is obtained by the finite element analysis of the magnetic field under different input current. Theoretical analysis is carried out to estimate the output torque of MRFDC according to the geometric dimensions of MRFDC structure and rheological properties of MRF. The Herschel-Bulkley model is applied to describe the MRF behaviour because the shear rate of MRF is relatively high. The output torque model is built considering the magnetic flux density. Therefore, the relationship between the transmissible torque and applied input current is determined. Finally, the MRFDC model is experimentally verified on the testbed; besides, the transmissible torque tests and response time tests for internal and external MRF clutches are carried out, respectively. The test results agree with the simulation results, and the differences are within 2 N m. It is suggested that the MRFDC can be applied in EVs to improve vehicle performance.

Keywords: magneto-rheological fluid, dual-clutch, finite element analysis, two-speed transmission, electric vehicles

(Some figures may appear in colour only in the online journal)

* Author to whom any correspondence should be addressed.

1. Introduction

The development of conventional internal combustion engine (ICE) vehicles significantly affects the social economy and human life. It provides significant convenience to people's lives but causes severe problems simultaneouly, e.g. high consumption of fossil fuel and environmental pollution [1–3]. Whereas EVs have advantages of high efficiency, simple powertrain, and zero emissions. Therefore, as the most promising means of transportation, EVs have been widely promoted by nations worldwide to substitute ICE vehicles to achieve energy conservation and environment protection [4, 5].

Since ICE can only operate in a very narrow speed range and requires idle speed, the ICE vehicles must be equipped with multi-speed transmission to realize wide speed range driving. Due to the torque and speed of ICE are challenging to control during the gear shifting process, a clutch between ICE and transmission is indispensable for start-ups, idle speed, and gear shifting. Compared to ICE, electric motors have the advantage of better controllability of torque and speed with good dynamic performance [6]. EVs are commonly equipped with only single-speed transmissions to trade off the complexity of the powertrain and cost on the market. Because of the increasing demands for higher efficiency and better performance, two-speed transmissions have been considered an alternative technology to improve EV's performance and reduce costs in the long term [7, 8].

The wide speed range for control provides EVs with an opportunity to simplify the transmissions. At present, many novel transmission structures for EVs are derived from traditional ones for ICE vehicles, e.g. inverse automated manual transmission [9], clutchless automated manual transmission (CLAMT) [10, 11], continuously variable transmission (CVT) [12, 13], and dual motor transmission [14], dual-clutch transmission (DCT) [15–17] and planetary transmission, clutchless [18–20]. Each kind of transmission has its advantages and disadvantages. CLAMT has less cost, higher efficiency, and more straightforward control than other transmissions. Nevertheless, torque interruption during the gear shifting process is significant and unavoidable. CVT provides a continuous transmission ratio and suffers from low torque transfer efficiency. Dual motor transmission solves the torque interruption problem by compensating the torque interruption during gear shifting with an extra motor. However, this structure brings about additional costs and complexity of design and control. DCT and planetary transmission have been validated to effectively compensate torque interruption through the clutch-to-clutch gearshift method [21, 22].

Magneto-rheological fluid (MRF) is a typical smart material composed of synthetic hydrocarbon or silicone oil and magnetic particles. The presence of a magnetic field can alter the viscosity of MRF sharply, causing the state of MRF to change from liquid to solid rapidly in milliseconds. The suspended magnetic particles become chain-like structures to resist shear deformation of the MRF flow under the influence of the magnetic field. MRF clutches are usually used as a torque transfer device. MRF clutch has many advantages compared with traditional hydraulic clutches, like quick response in milliseconds, controllable torque, compact structure, and low power consumption [23]. However, research papers on MRF clutches are few, especially for EV applications. Bucchi *et al* designed an MRF clutch with permanent magnets (PMs) to disengage the vacuum pump when the power brake of diesel engine vehicles does not need to work [24, 25]. The author also studied the effect of temperature on the torque characteristic of a PM MRF clutch [26]. Rizzo *et al* developed an innovative, effective, and fail-safe MRF-based clutch [27]. They proposed a multi-gap PM clutch-based MRF to reduce torque loss in the disengagement process [28]. His research group proposed another innovative multi-gap clutch based on MRF [29]. The electromagnetic torque generated by the interaction between eddy currents and the magnetic field improves the clutch's performance. However, the transmissible torque of the above MRF clutch is minimal and is used for mechanical actuation, not for vehicle application. Daoming Wang *et al* proposed a novel MRF clutch applied in vehicle powertrain systems and studied the transient temperature field's distribution, variation and impact factors [30]. However, the torque transfer capability is not analysed.

In this study, a new type of powertrain with MRF dual-clutch (MRFDC) of EVs is proposed by combining DCT and MRF clutch [31]. The main contribution of this paper is to develop a new type of MRFDC that can be applied in EVs with two-speed transmissions. This paper focuses on the design, analysis and test of the MRFDC with the two-speed transmission for EVs. The following parts will present the design details, working principle, torque estimation, and experimental tests.

2. Structure design and working principle of MRFDC

2.1. The structure design of MRFDC

Typically, MRF clutches have two standard layouts [32]. One layout is a disk-shaped MRF clutch, and the other layout is a drum-shaped MRF clutch. The two types of structures are shown in figure 1. To satisfy the requirement of space limitation, a multi-gaps MRFDC is adopted in this study and torque transmission by combining the disc-shaped and drum-shaped clutches [33]. The schematic diagram of MRFDC is shown in figure 2.

The proposed clutch contains an internal MRF clutch and an external MRF clutch. The two clutches can transfer torque independently. As shown in figure 2, the red and green parts consist of the internal clutch. In comparison, the red and the yellow parts consist of the external clutch. The internal clutch has a drum-shaped structure because it should have a smaller radial dimension under space constraints. However, the external clutch has a disk-shaped structure because it should have a more straightforward structure under the output torque and space limitation requirement.

As shown in figure 1, the MRFDC is supported by bearing 1 and bearing 2, mounted on the input shaft and output shaft 2 of MRFDC. Output shaft 1 is supported by bearing 3 and bearing 4, connecting with the first gear. While output

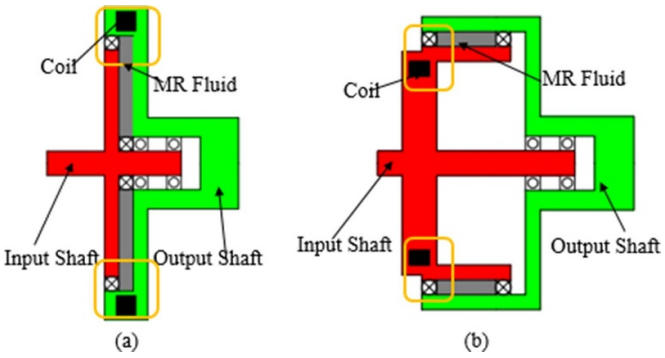

Figure 1. (a) Configuration of the disc-type MRF clutch. (b) Configuration of the drum-type MRF clutch.

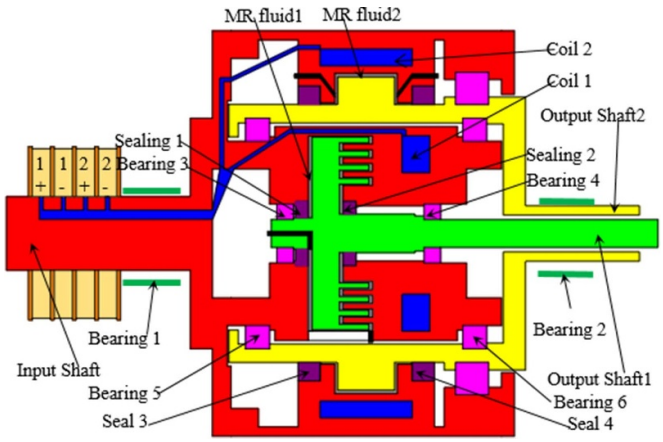

Figure 2. Schematic diagram of MRFDC.

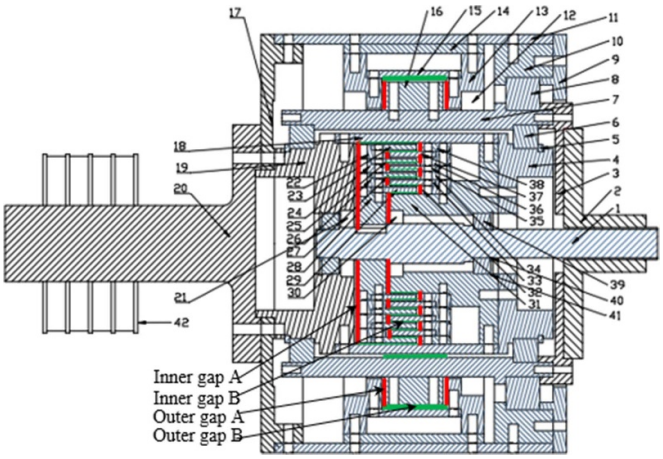

Figure 3. Assembly drawing of MRFDC.

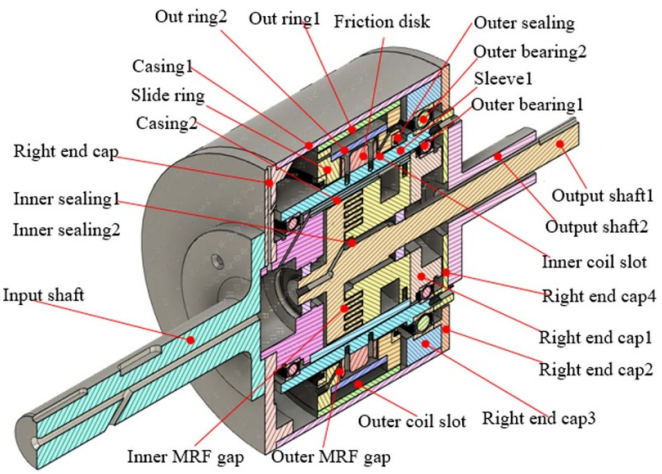

Figure 4. 3D model of MRFDC.

shaft 2 is supported by bearing 5 and bearing 6, connecting with the second gear. Nitrile seals are employed to prevent leakage of MRF, shown in purple colour. MRF is filled in all gaps of the MRFDC in this structure, as shown in grey colour. There are two reserved holes for each clutch to fill the MRF, shown in black colour. The coils are shown in cyan colour in figure 2. In this design, all fluid gaps are exposed to the magnetic field. The magnetic induction line can pass through all MRF gaps, and magnetic flux density is considered constant in the radial direction. Both coils can rotate when the clutch is working. To not get entangled when the MRFDC is working, the coils are connected with a rotating conductive ring that contacts the fixed brushes. The circuit is shown in blue colour. A four-wire connector connects the positive and negative electrodes of the internal and external clutch, respectively. The assembly drawing and 3D model of the MRFDC are shown in figures 3 and 4.

Some critical parameters of the proposed clutch used in this paper are summarized in table 1. The diameter of the coil is 0.5 mm. Inner and outer MRF Gaps A and B in table 1 are the radial and tangential direction gaps. As shown in figure 3, gaps A are shown in red, and gaps B are shown in green. Figure 4 shows the 3D model of MRFDC. The dimension of length, width and height of the designed MRFDC is 324 mm, 220 mm and 220 mm, respectively. The total weight is about 10.2 kg.

The clutch includes some main components, such as disks, drums, MRF, coils, and housing, and the part list is shown in table 2. The disc and the drum filled with MRF are manufactured by low carbon steel because it has high magnetic permeability. Stainless steel bearings and the nitrile seal have non-magnetic property. The rest are mainly made of 6060 aluminium because it has low material density and low magnetic permeability. The MRF-132-DG is adopted since it has a millisecond-level fast response time and wide controllability of magnetic field intensity. Table 3 shows the relative magnetic permeability of all materials. Different structures and materials can guide the magnetic flux in the desired way with minimal leakage.

2.2. *Working principle of MRFDC*

The physical map of MRFDC and two-speed transmission gears is shown in figure 5. The transmission consists of two rows of planetary gears which share the same outer ring gear. Two sun gears with different radius are installed on the same

Table 1. Characteristic design parameters of the MRFDC.

	Inner MRF gap size (mm)		Outer MRF gap size (mm)			
Thickness (mm)	A	B	A	B	Coils turn C1	Coils turn C2
30	1	0.75	1	2	3000	1200

Table 2. Part list of MRFDC.

Part list			
Item	Qty	Part name	Material selection
1	1	Output shaft1	6061 aluminium
2	1	Output shaft2	6061 aluminium
3	1	Right end cap1	6061 aluminium
4	1	Right end cap2	6061 aluminium
5	2	Retaining ring1	65 Mn
6	2	Outer bearing1	Stainless steel
7	1	Sleeve1	6061 aluminium
8	1	Outer bearing2	Stainless steel
9	1	Right end cap3	6061 aluminium
10	1	Right end cap4	6061 aluminium
11	1	Casing1	6061 aluminium
12	2	Outer sealing 140 × 160 × 12	Nitrile
13	2	Side ring	Low carbon steel
14	1	Out ring1	Low carbon steel
15	1	Our ring2	6061 aluminium
16	1	Friction disk	Low carbon steel
17	1	Left end cap1	6061 aluminium
18	1	Casing2	Low carbon steel
19	1	Left end cap2	6061 aluminium
20	1	Input Shaft	6061 aluminium
21	1	Inner Sealing1	Nitrile
22	1	Left ring connector1	6061 aluminium
23	1	Inner left ring1	Low carbon steel
24	1	Left ring connector2	6061 aluminium
25	1	Inner left ring2	Low carbon steel
26	1	Left ring connector3	6061 aluminium
27	1	Inner left ring3	Low carbon steel
28	1	Left ring connector4	6061 aluminium
29	1	Inner left ring4	Low carbon steel
30	1	Inner Sealing2	Nitrile
31	1	Inner clutch housing	Low carbon steel
32	1	Right ring connector1	6061 aluminium
33	1	Inner right ring1	Low carbon steel
34	1	Right ring connector2	6061 aluminium
35	1	Inner ring ring2	Low carbon steel
36	1	Right ring connector3	6061 aluminium
37	1	Inner right ring3	Low carbon steel
38	1	Right ring connector4	6061 aluminium
39	2	Inner bearing	Stainless steel
40	2	Retaining ring1	65 Mn
41	2	Retaining ring2	65 Mn
42	1	Conductive ring	Copper

Table 3. Relative magnetic permeability.

Material	Relative magnetic permeability
Low carbon steel	1000
6060 Al	1
Air	1
Coil	1
Stainless steel	1
Nitrile	1
MRF-132-DG	3.73

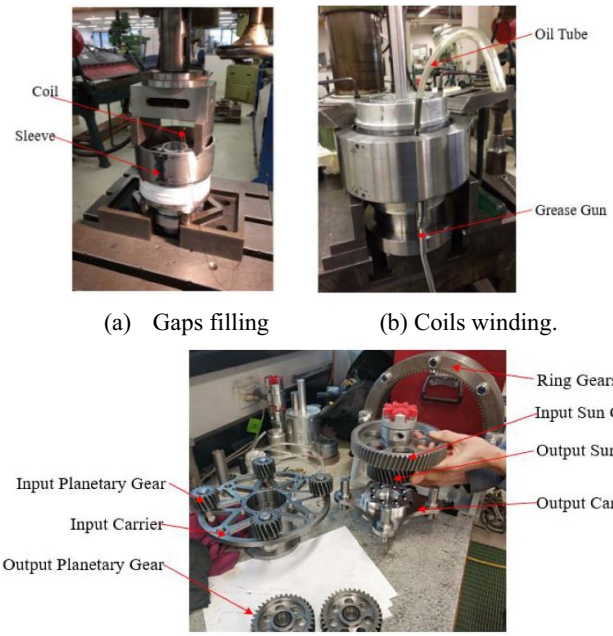

(a) Gaps filling (b) Coils winding.

(c) Planetary gears

Figure 5. Physical map of MRFDC and two-speed transmission gears.

shaft. Four same planetary gears are mounted between the ring gear and sun gear. Due to input and output planetary gears have different sizes. Different gear ratios can be obtained in various combinations. For the first gear, outshaft1 connects the internal MRF clutch and the input shaft of the sun gear in this design. While for the second gear, outshaft2 connects the external MRF clutch and the input shaft of the carrier. Both gears had the same output shaft, which is connected with the load.

The working principle diagram is shown in figure 6. The coli energized by the input current will generate a magnetic field, and the MRF in the gaps will immediately become solid. The shear stress between the rotating drum and the solidified MRF provides the transmissible torque to connect the input shaft and the output shaft. Specifically, when the first gear operates, the input current is applied to the internal clutch coil, and no current is applied to the external clutch coil. The internal clutch will be engaged, while the external clutch will be disengaged simultaneously. Therefore, the MRFDC

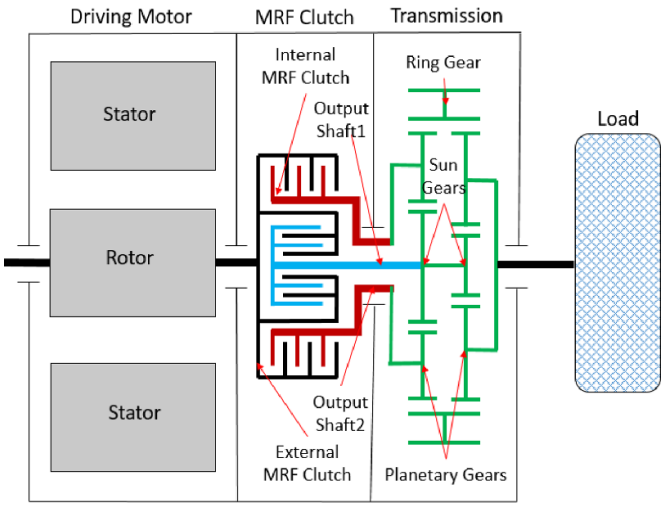

Figure 6. Working principle diagram of MRFDC.

can transfer the torque from the EM to output shaft1. During the process of upshifting, the current through the internal clutch coil gradually decreases to zero. In contrast, the current through the external clutch coil gradually increases to a specific value simultaneously. The external clutch starts to be engaged, while the internal clutch is disengaged in the meantime. Upshifting is realized by the torque being dynamically transferred from the internal clutch to the external clutch by controlling the input current. Consequently, the torque can be transferred from the EM to output shaft 2 smoothly.

3. Transmissible torque analysis

3.1. Theoretical analysis

In this section, transmissible torque is analysed theoretically. The relationship between the transmissible torque and the applied current is obtained firstly. The relationship can be divided into two parts. The first part is the relationship between the output torque and the magnetic field, while the second part is the relationship between the magnetic field and the applied current. The output torque has to be estimated according to the magnetic field firstly.

The derivation of the transmissible torque of the external MRF clutch is only presented in this paper because it is similar to that of the internal MRF clutch. The transmissible torque of the external MRF clutch generally comes from two parts. One part is the friction torque between the MRF in the radial direction and the end face of the disc (section 1), and the other part is the friction torque between the MRF in the annular duct in the circumferential direction and the outer cylinder of the disc (section 2). The principal geometric sizes of the external MRF clutch are demonstrated in figure 7.

As shown in figure 8, taking a small annular ring element of MRF in the gap between the sleeve and the disc, the friction torque acting on the element can be defined as follows [34]:

$$\mathrm{d}T = 2\pi r^2 \tau_z \mathrm{d}r + 2\pi r^2 \tau_r \mathrm{d}z. \tag{1}$$

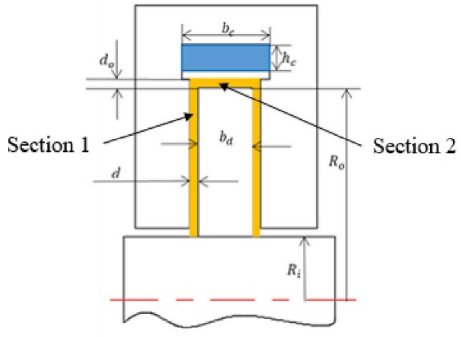

Figure 7. Principal dimensions of the novel MRFDC.

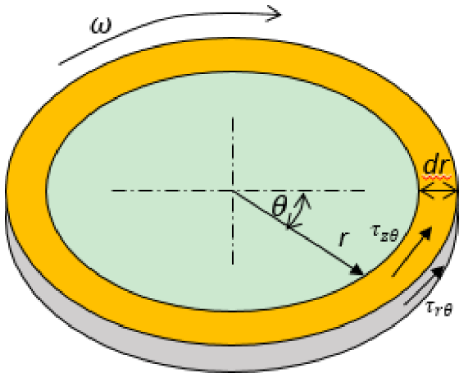

Figure 8. Annular ring element of MRF in the gap.

The friction torque generated by the MRF in sections 1 and 2 can be calculated, respectively, as follows:

$$T_1 = 2\pi \int_{r_i}^{r_o} r^2 \tau_z \mathrm{d}r + 2\pi \int_{r_o}^{r_o+d_o} r^2 \tau_z \mathrm{d}r \tag{2}$$

$$T_2 = 2\pi {r_o}^2 \int_0^d \tau_r \mathrm{d}z + 2\pi {r_o}^2 \int_0^{b_d} \tau_r \mathrm{d}z. \tag{3}$$

The fluid gap size d_o and d are minimal compared to the radial dimension $(r_o - r_i)$ and thickness (b_d), respectively. Hence, the second term in equations (2) and (3) can be ignored, then equations (2) and (3) can be rewritten as follows:

$$T_1 = 2\pi \int_{r_i}^{r_o} r^2 \tau_z \mathrm{d}r \tag{4}$$

$$T_2 = 2\pi {r_o}^2 \int_0^{b_d} \tau_r \mathrm{d}z. \tag{5}$$

The constitutive Herschel-Bulkley model of MRF is adopted to model the MRF behaviour. It can predict the MRF behaviour precisely under high shear rate conditions [34]. The

Herschel-Bulkley model in the circumferential direction can be mathematically described as the following equation:

$$\tau = \tau_y + K\dot{r}^n \tag{6}$$

where τ and τ_y represent the shear stress and yield stress of the MRF, respectively. The exponent n represents the flow behaviour index and K represents the consistency. $\dot{r}$ is the shear rate of the MRF and can be approximately described as follows:

$$\dot{\gamma} = \frac{r\omega}{d} \text{ (section 1)} \tag{7}$$

$$\dot{\gamma} = \frac{r_o\omega}{d_o} \text{ (section 2)}. \tag{8}$$

Substituting equations (6)–(8) into equations (4) and (5), respectively, the transmissible torque generated by the friction of the MRFDC can be determined as follows:

$$T_1 = 2\pi \int_{r_i}^{r_o} r^2\tau_y \mathrm{d}r + 2\pi \int_{r_i}^{r_o} r^2 K \left(\frac{r\dot{\theta}}{d}\right)^n \mathrm{d}r \tag{9}$$

$$T_2 = 2\pi {r_o}^2 \int_0^{b_d} \tau_y \mathrm{d}z + 2\pi {r_o}^2 \int_0^{b_d} K_0 \left(\frac{r_0\dot{\theta}}{d_0}\right)^{n_0} \mathrm{d}z. \tag{10}$$

where n_0 and K_0 are the MRF behaviour index and the consistency of the MRF under zero magnetic field. In section 2, the magnetic flux density across the annular duct of MR fluid is minimal, and the yield stress in the annual duct can be neglected. Then, the total transmissible torque T_t can be calculated as follows:

$$T_t = 2T_1 + T_2 = 4\pi \int_{r_i}^{r_o} r^2\tau_y \mathrm{d}r + 4\pi \int_{r_i}^{r_o} r^2 K \left(\frac{r\dot{\theta}}{d}\right)^n \mathrm{d}r + 2\pi {r_o}^2 \int_0^{b_d} K_0 \left(\frac{r_0\dot{\theta}}{d_0}\right)^{n_0} \mathrm{d}z. \tag{11}$$

To calculate the transmissible torque conveniently, the magnetic density is assumed to be constant without respect to variation in the function of r. The values of τ_y, K and n are also constants. Then equation (11) can be analytically calculated by integral as follows:

$$T_t = \frac{4\pi\tau_y}{3}\left({r_o}^3 - {r_i}^3\right) + \frac{4\pi\mu_{eq}{r_o}^4}{(n+3)\,d}\left[1 - \left(\frac{r_i}{r_o}\right)^{n+3}\right]\dot{\theta} + 2\pi {r_o}^2 b_d K_0 \left(\frac{r_0\dot{\theta}}{d_0}\right)^{n_0} \tag{12}$$

where $\mu_{eq} = K\left({}^{r_o\omega}/_{d}\right)^{n-1}$ is the equivalent viscosity of the MRF. When no input current is applied to the coil, the transmissible torque (under zero magnetic field condition) can be expressed as follows:

$$T_{t,0} = \frac{4\pi\mu_{eq,0}{r_o}^4}{(n_0+3)\,d}\left[1 - \left(\frac{r_i}{r_o}\right)^{n_0+3}\right]\dot{\theta} + 2\pi {r_o}^2 b_d K_0 \left(\frac{r_0\dot{\theta}}{d_0}\right)^{n_0} \tag{13}$$

where $\mu_{eq} = K_0\left({}^{r_o\omega}/_{d}\right)^{n_0-1}$ is the equivalent viscosity of the MRF under zero magnetic field condition.

The estimation of rheological properties of the MRF such as the yield stress τ_y, flow behaviour index n and fluid consistency K is first conducted. The rheological properties of the MRF are related to the magnetic flux density generated by the input current and can be described by the following equation [35]:

$$Y = Y_\infty + (Y_0 - Y_\infty)\left(2e^{-B\alpha_{SY}} - e^{-2B\alpha_{SY}}\right) \tag{14}$$

where Y, Y_0 and Y_∞ represent the rheological property parameters of MRF, the value under zero magnetic field condition and the saturation value of the rheological property parameters, respectively. B represents the magnetic flux density. α_{SY} represents the saturation moment index of the parameter Y. The parameters, Y_0, Y_∞ and α_{SY} can be determined based on the experimental results using a method by curve fitting [36]. In this paper, MRF-132-DG made by Lord Corp is adopted considering the property and price. Its rheological property parameters under zero magnetic field and saturation conditions are obtained experimentally and shown in table 4.

Table 4. Rheological properties of MRF-132-DG.

Parameter	Value
K_0	0.22 Pa s^n
K_∞	3900 Pa s^n
α_{sk}	5 T^{-1}
τ_{y0}	10 Pa
$\tau_{y\infty}$	30 000 Pa
α_{st_y}	2 T^{-1}
n_0	0.917
n_∞	0.25
α_{sn}	32

Substituting the rheological property parameters in equation (14) into equations (12) and (13), we can obtain the relationship between the transmissible torque and the magnetic flux density of the MRFDC.

3.2. Simulation

In this section, the relationship between the magnetic and the applied input current is obtained. Finite element analysis (FEA) of the magnetic field of MRFDC is carried out using ANSYS Mechanical APDL 15.0 [37]. The FEM of the MRFDC is shown in figure 9. Materials with different relative magnetic permeability are shown in different colour. MRF is shown in orange colour. The magnetic flux density is obtained during the analysis under applied input current from 0.1 A to 1.0 A with 0.1 A space.

Figures 10–13 show the magnetic induction lines and magnetic flux density distribution of the internal and external

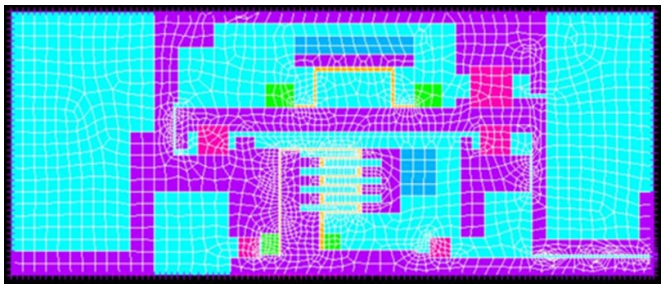

Figure 9. Finite element model of MRF dual-clutch.

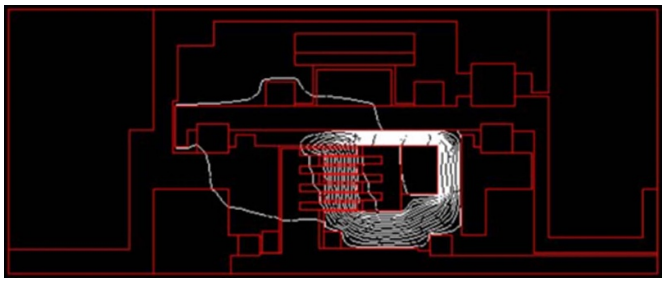

Figure 10. Magnetic induction line of internal MRF clutch with 1.0 A current.

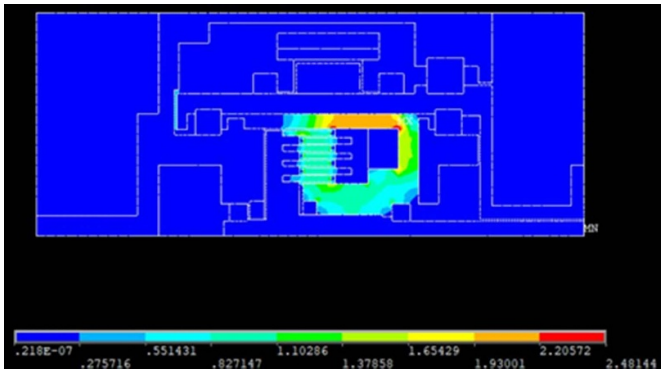

Figure 11. Magnetic flux density distribution of internal MRF clutch with 1.0 A current.

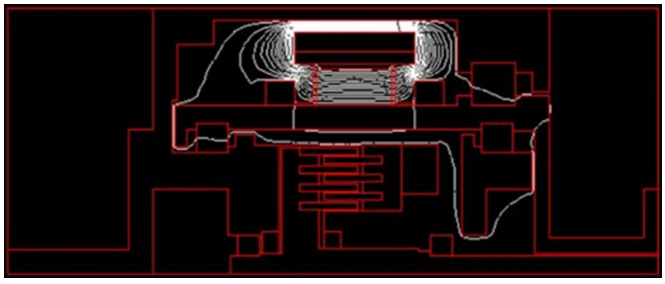

Figure 12. Magnetic induction line of external MRF clutch with 1.0 A current.

MRF clutch with the input current of 1.0 A, respectively. Figures 10 and 12 show that some magnetic induction lines leakage because of errors in design and assembly. However, the leakage is insignificant and can be ignored.

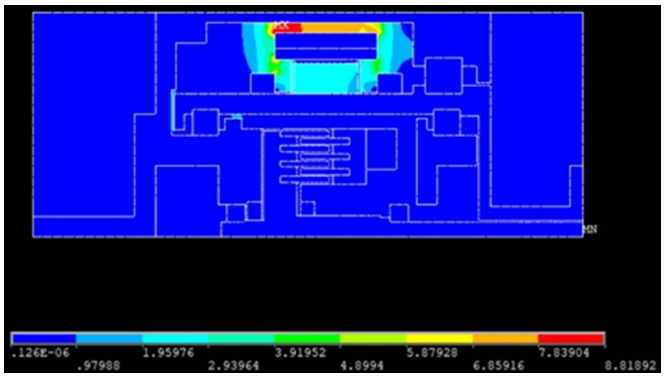

Figure 13. Magnetic flux density distribution of external MRF clutch with 1.0 A.

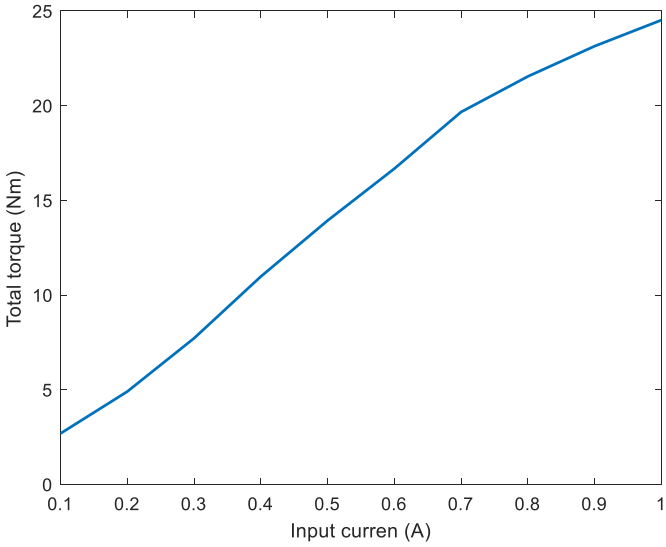

Figure 14. Output torque versus input current of internal clutch.

The magnetic flux density B is determined by the average value of the magnetic flux density at the centre points of MRF gaps. The FEA of the transmissible torque for the MRFDC can be used to verify the experimental results verification. The relationship between the transmissible torque and the input current for the internal and external MRF clutch are shown in figures 14 and 15, respectively. As shown in figure 14, the total transmissible torque can achieve 24.5 N m when the input current of the internal MRF clutch reaches 1 A. However, the total transmissible torque of external MRF can achieve 52.9 N· m under the same condition., shown in figure 15.

4. Experimental verification

4.1. Experimental setup

A testbed is established to verify the performance of the MRFDC. The schematic diagram of the testbed is shown in figure 16. Red lines show the electric signal flow, and black lines show mechanical connections. The testbed consists of a computer, a real-time control board (Model: myRIO-1990), a battery, a motor, a motor controller, a reducer, the designed

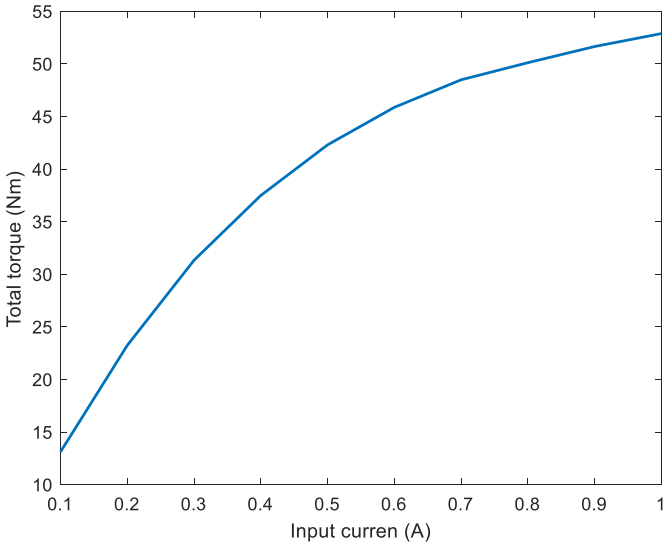

Figure 15. Output torque versus input current of external clutch.

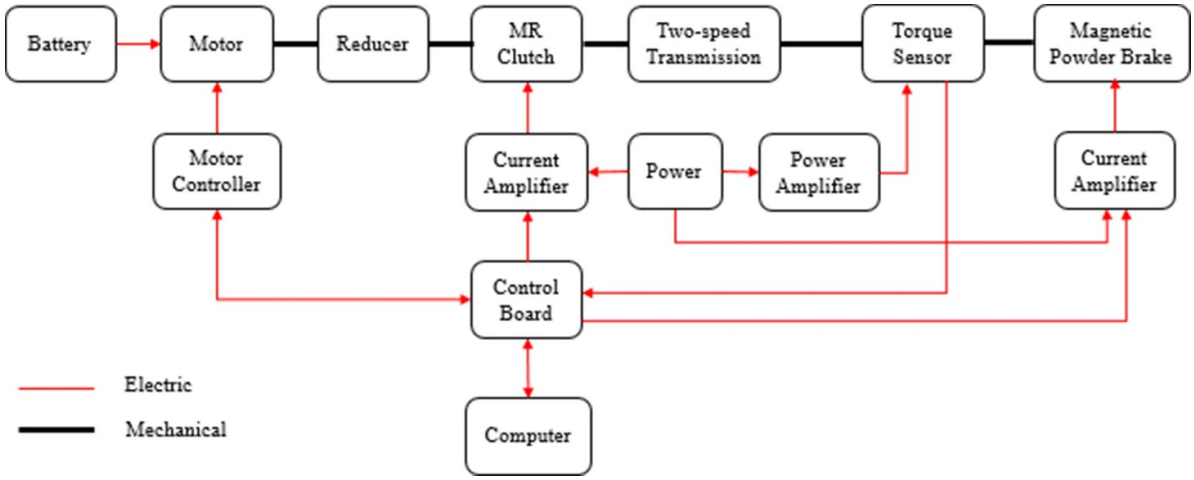

Figure 16. Schematic program of the MR clutch test rig.

MRFDC, a torque sensor, a power amplifier, three current amplifiers, a magnetic power brake and a cooling water pump as shown in figure 16 Schematic program of the MR clutch test rig. The physical diagram is shown in figure 17.

In the test system, LABVIEW software is utilized to record test data and write the system test program. The program implemented in myRIO sends command signals and acquires test data. As it can be seen from figure 16, the myRIO sends the speed command signal to the motor controller and the current command signal to the current amplifier to deliver the MRFDC signal and magnetic power brake signal command, respectively. The myRIO also can receive the transmissible torque signal from the torque sensor.

The speed control of the motor can be realized by the Proportion Integration Differentiation (PID) control algorithm implemented in the motor controller. A 3 kw permanent magnet synchronous motor and a torque sensor with the maximum range of 500 N m are adopted.

The torque sensor is powered by a power amplifier. The characteristic curve of the driving motor is shown in figure 18. The rated speed and torque is 4000 rpm and 10 N m, respectively. A reducer with a ratio of 16 is utilized to reduce the output speed and increase the motor's output torque. The current amplifier can control the magnetic field in MRFDC and the magnetic powder brake by the control current according to the command signal from myRIO. Thus the transmissible torque and loading torque can be controlled. The relationship between the input current and the transmissible torque of the MRFDC can be acquired by test data.

4.2. Torque test under zero-magnetic field

Before the first test, the motor rotates at the speed of 60 rpm for 2 min without any input current so that the particles suspended in MRF are evenly distributed. In the first test, the transmissible torque of the MRFDC under zero-magnetic field at different input speeds is tested. The MRFDC is considered to work at the idling state when no current is applied to the coils.

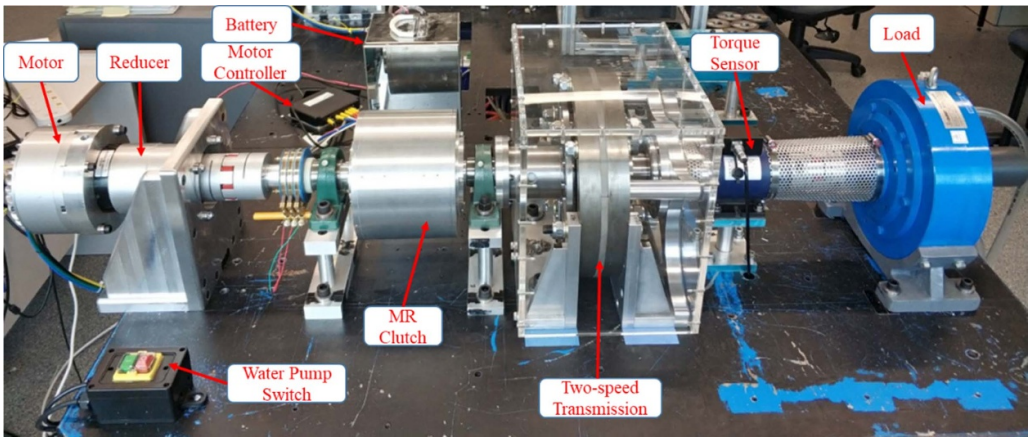

Figure 17. Testbed.

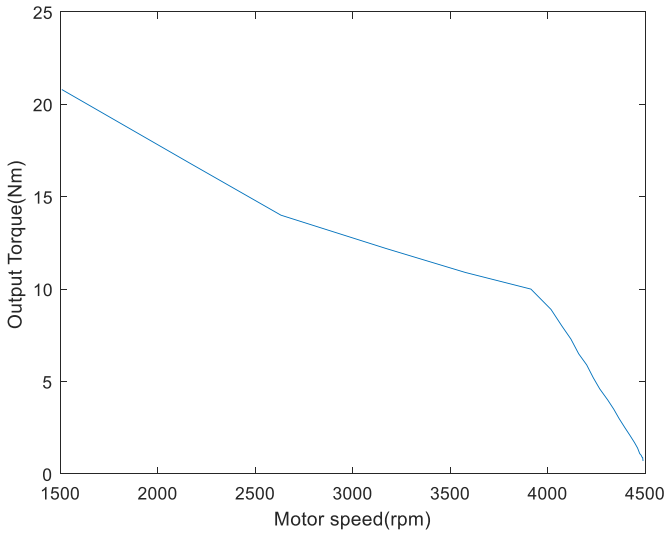

Figure 18. Characteristic curve of driving motor.

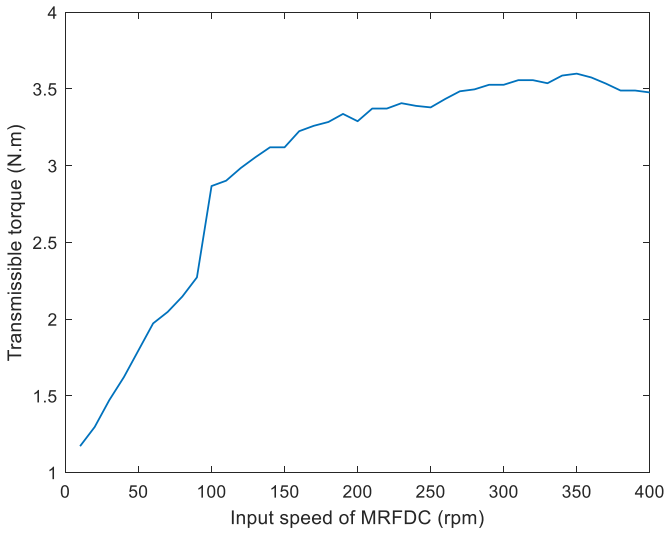

Figure 19. Measured transmissible torque at different clutch input speeds under zero-magnetic field.

The motor rotates at a constant speed and runs for 20 s during each test. Hence the MRF temperature is assumed not to change too much during this period. The transmissible torque of the MRFDC under a zero-magnetic field is also called drag torque. The relationship between the drag torque and input speed of MRFDC is shown in figure 19. The drag torque is mainly caused by MRF viscous shear. It is also affected by input and output speed difference of MRFDC, temperature, rheological properties of MRF and the structure design of MRFDC [15]. The drag torque increases as the input speed of MRFDC increases, and it tends to be stable when the speed reaches 200 rpm. The test results show that the drag torque is no more than 4 N m, far less than the actual engaged transmissible torque.

4.3. Response time and transmissible torque test

In the second test, the response time and transmissible torque of the MRFDC are tested, respectively. During the tests, the motor rotates at the speed of 120 rpm. Firstly, the input current of 0.5 A and 0.8 A is applied to the internal MRF clutch coils, respectively, at the 1st second. As shown in figures 20 and 21, the measured response time of the internal MRF clutch reaches approximately 152 ms and 126 ms, respectively. The step response time of the proposed system can be determined by the time required for the response value to reach 63.2% of the steady-state value. The responding speeds of MRFDC are much faster than that of a traditional clutch (200–300 ms) [38]. Hence, gearshifting time will be much shortened using this MRFDC. The measured torque is 13 N m and 22 N m, respectively. These test results are close to the simulation results (13.9 N m and 21.5 N m, as shown in figure 14).

Secondly, the input current of 0.5 A and 0.8 A current is applied to the external MRF clutch coils, respectively, at the 1st second. As shown in figures 22 and 23, the measured response time of the external MRF clutch reaches about 134 ms and 152 ms, respectively, and the measured transmissible torque reaches about 40.7 N m and 50.1 N m.

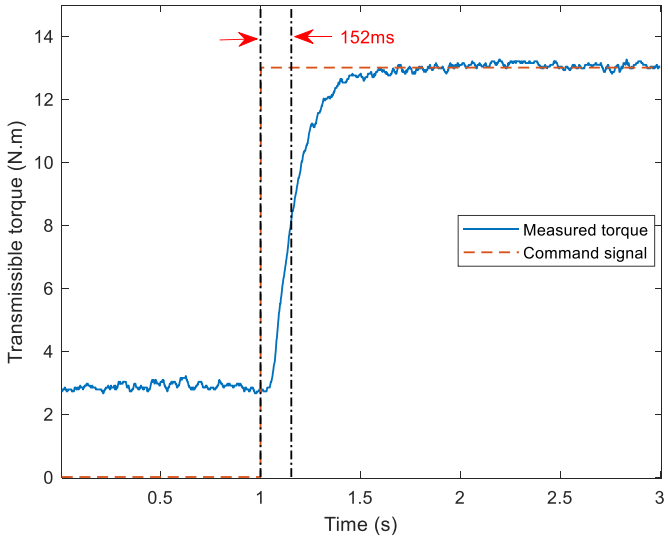

Figure 20. Measured response time and transmissible torque of the internal clutch under 0.5 A current excitation.

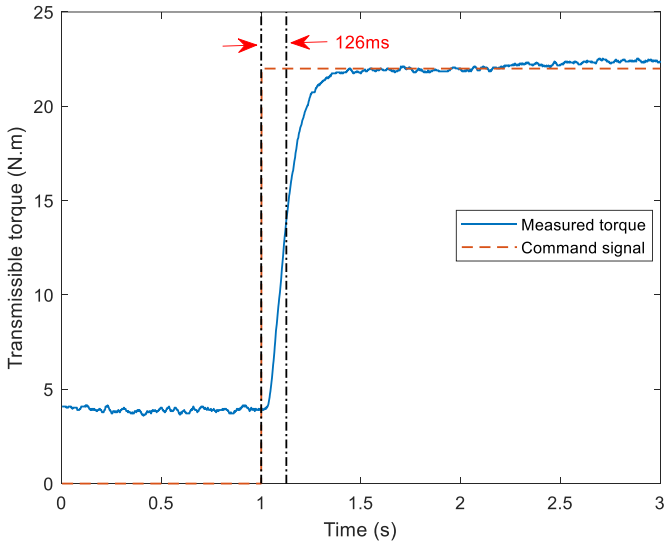

Figure 21. Measured response time and transmissible torque of the internal clutch under 0.8 A current excitation.

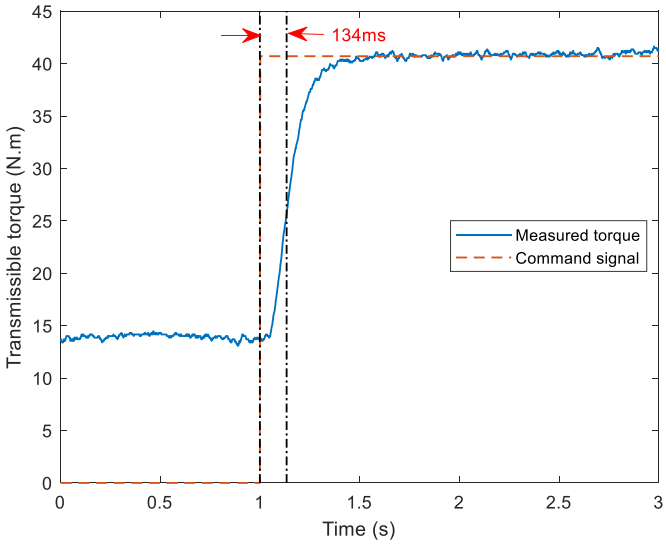

Figure 22. Response time and transmissible torque of the external clutch under 0.5 A current excitation.

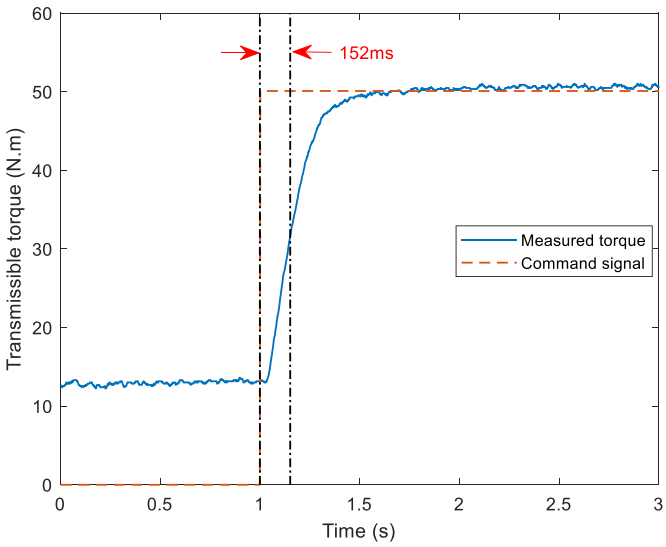

Figure 23. Response time and transmissible torque of the external clutch under 0.8 A current excitation.

The measured results are consistent with the simulation results (42.3 N m and 50.1 N m, shown in figure 15). To compare the simulation data and experimental results more accurately, 0.2 A, 0.4 A, 0.6 A, 0.8 A, and 1 A current are applied to the internal and external MRF clutch, respectively.

4.4. Discussion

Measured transmissible torque versus simulated transmissible torque for the internal MRF clutch and external MRF clutch are shown in figures 24 and 25, respectively. As figures 24 and 25 show, the measured transmissible torque of the internal MRF clutch can reach 25.6 N m when the clutch is applied 1 A input current. In comparison, the measured transmissible torque of the external MRF clutch can reach 54.1 N m when the clutch is applied 1 A input current. During the test in the lab, the maximum transmissible torque can reach 36.3 N m and 60.7 N m for internal and external MRF clutch when the input current reaches 2.3 A and 1.4 A, respectively. The fitting curve shape of the experimental results is coincident with that of the simulation results. However, there are some differences between the two fitting curves. The differences are with 2 N m because the friction caused by the installation error of MRFDC is not considered when FEA is conducted. In addition, there are some errors when the magnetic flux density at the centre point of MRF gaps is used as a calculated value. Hence, considering all the above factors, the simulation results agree well with the experimental results, proving that the theoretical and simulation methods are reasonable.

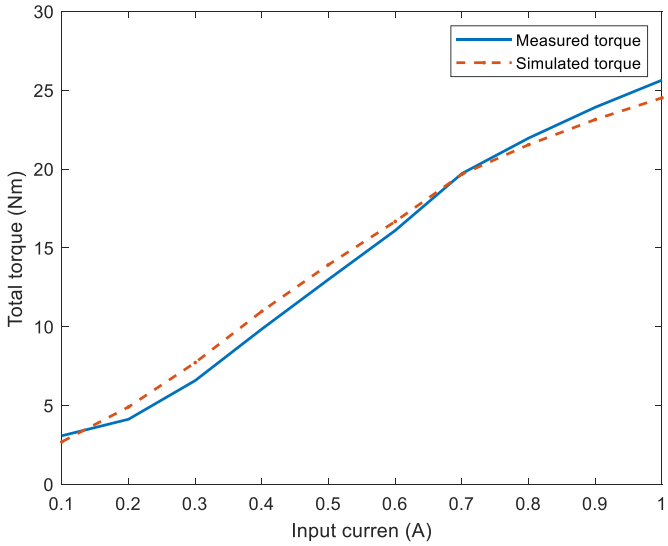

Figure 24. Measured transmissible torque versus simulated transmissible torque for internal MRF clutch.

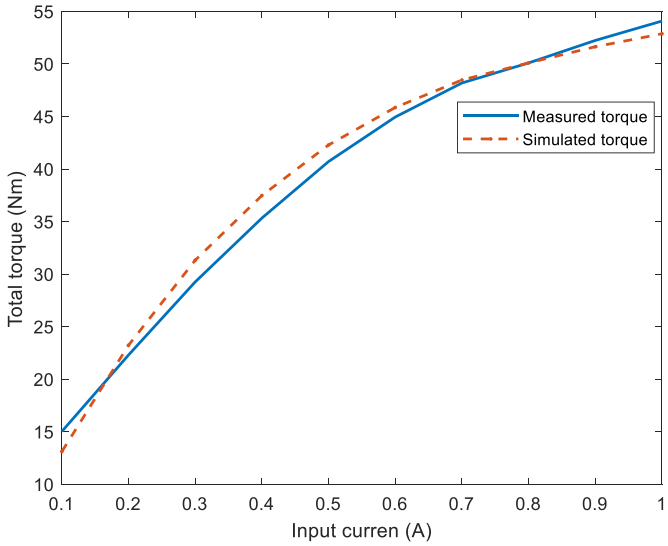

Figure 25. Measured transmissible torque versus simulated transmissible torque for external MRF clutch.

5. Conclusions

In this paper, a novel MRFDC has been presented for EVs with two-speed transmissions. The structure design of MRFDC is inspired by the MRF clutch and traditional DCT by combining their advantages to achieve high control accuracy and fast response speed. The design details and working principles of MRFDC have been introduced. FEA has been carried out to obtain the relationship between the input current and magnetic fields. Also, the relationship between transmissible torque of the MRF clutch and the input current has been obtained according to the geometric dimensions of the MRFDC structure, rheological properties of MRF, and the input current. Experiments have been carried out to validate the performance of the developed device. Transmissible torque under zero-magnetic field and response time with energized coils have been obtained by tests. The experimental results show that the proposed MRFDC can achieve high controllable torque and fast response, indicating the feasibility of the MRFDC in EVs.

The structural optimization of MRFDC will be conducted to improve the transmissible torque, and advanced controllers will be developed to guarantee the system performance.

Data availability statement

The data that support the findings of this study are available upon reasonable request from the authors.

Acknowledgments

This research is supported by the Australian Research Council Linkage Project Grant (LP190100603), and the University of Wollongong and China Scholarship Council (CSC) joint scholarship.

ORCID iDs

Huan Zhang https://orcid.org/0000-0001-6531-8886
Shuaishuai Sun https://orcid.org/0000-0002-8695-9217
Donghong Ning https://orcid.org/0000-0001-9905-4575
Weihua Li https://orcid.org/0000-0002-6190-8421

References

[1] Li L, You S, Yang C, Yan B, Song J and Chen Z 2016 Driving-behavior-aware stochastic model predictive control for plug-in hybrid electric buses *Appl. Energy* **162** 868–79
[2] Reitz R *et al* 2020 IJER Editorial: The Future of the Internal Combustion Engine *Internal Journal of Engine Research* **21** 3–10
[3] Sher E 1998 Handbook of Air Pollution from Internal Combustion Engines: Pollutant Formation and Control (New York: Academic) (https://doi.org/10.1016/B978-0-12-639855-7.X5038-8)
[4] Martinez C M, Hu X, Cao D, Velenis E, Gao B and Wellers M 2016 Energy management in plug-in hybrid electric vehicles: recent progress and a connected vehicles perspective *IEEE Trans. Veh. Technol.* **66** 4534–49
[5] Ahmadi P 2019 Environmental impacts and behavioral drivers of deep decarbonization for transportation through electric vehicles *J. Clean. Prod.* **225** 1209–19
[6] Hu X, Zou C, Zhang C and Li Y 2017 Technological developments in batteries: a survey of principal roles, types, and management needs *IEEE Power Energy Mag.* **15** 20–31
[7] Sorniotti A *et al* 2012 Analysis and simulation of the gearshift methodology for a novel two-speed transmission system for electric powertrains with a central motor *Proc. Inst. Mech. Eng.* D **226** 915–29
[8] Zhu B, Zhang N, Walker P, Zhan W, Zhou X and Ruan J 2013 Two-speed DCT electric powertrain shifting control and rig testing *Adv. Mech. Eng.* **5** 323917
[9] Gao B, Liang Q, Xiang Y, Guo L and Chen H 2015 Gear ratio optimization and shift control of 2-speed I-AMT in electric vehicle *Mech. Syst. Signal Process.* **50** 615–31
[10] Tseng C-Y and Yu C-H 2015 Advanced shifting control of synchronizer mechanisms for clutchless automatic manual transmission in an electric vehicle *Mech. Mach. Theory* **84** 37–56

[11] Walker P D, Fang Y and Zhang N 2017 Dynamics and control of clutchless automated manual transmissions for electric vehicles *J. Vib. Acoust.* **139** 061005

[12] Hofman T and Dai C 2010 Energy efficiency analysis and comparison of transmission technologies for an electric vehicle *2010 IEEE Vehicle Power and Propulsion Conf.* (IEEE) pp 1–6

[13] Sorniotti A, Subramanyan S, Turner A, Cavallino C, Viotto F and Bertolotto S 2011 Selection of the optimal gearbox layout for an electric vehicle *SAE Int. J. Eng.* **4** 1267–80

[14] Liang J, Yang H, Wu J, Zhang N and Walker P D 2018 Power-on shifting in dual input clutchless power-shifting transmission for electric vehicles *Mech. Mach. Theory* **121** 487–501

[15] Zhou X, Walker P, Zhang N, Zhu B and Ruan J 2014 Numerical and experimental investigation of drag torque in a two-speed dual clutch transmission *Mech. Mach. Theory* **79** 46–63

[16] Hong S, Son H, Lee S, Park J, Kim K and Kim H 2016 Shift control of a dry-type two-speed dual-clutch transmission for an electric vehicle *Proc. Inst. Mech. Eng.* D **230** 308–21

[17] Walker P, Zhu B and Zhang N 2017 Powertrain dynamics and control of a two speed dual clutch transmission for electric vehicles *Mech. Syst. Signal Process.* **85** 1–15

[18] Fang S, Song J, Song H, Tai Y, Li F and Nguyen T S 2016 Design and control of a novel two-speed uninterrupted mechanical transmission for electric vehicles *Mech. Syst. Signal Process.* **75** 473–93

[19] Mousavi M S R, Pakniyat A, Wang T and Boulet B 2015 Seamless dual brake transmission for electric vehicles: design, control and experiment *Mech. Mach. Theory* **94** 96–118

[20] Tian Y, Ruan J, Zhang N, Wu J and Walker P 2018 Modelling and control of a novel two-speed transmission for electric vehicles *Mech. Mach. Theory* **127** 13–32

[21] Lee S, Zhang Y, Jung D and Lee B 2014 A systematic approach for dynamic analysis of vehicles with eight or more speed automatic transmission *J. Dyn. Syst. Meas. Control* **136** 051008

[22] Mishra K D and Srinivasan K 2017 Robust control and estimation of clutch-to-clutch shifts *Control Eng. Pract.* **65** 100–14

[23] Zhang H, Du H, Sun S, Li W and Wang Y 2019 Design and analysis of a novel magnetorheological fluid dual clutch for electric vehicle transmission SAE Technical Paper 0148–7191

[24] Bucchi F, Forte P, Frendo F and Squarcini R 2013 A magnetorheological clutch for efficient automotive auxiliary device actuation *Frattura. Integr. Strutt.* **7** 62–74

[25] Bucchi F, Forte P, Frendo F, Musolino A and Rizzo R 2014 A fail-safe magnetorheological clutch excited by permanent magnets for the disengagement of automotive auxiliaries *J. Intell. Mater. Syst. Struct.* **25** 2102–14

[26] Bucchi F, Forte P and Frendo F 2015 Temperature effect on the torque characteristic of a magnetorheological clutch *Mech. Adv. Mater. Struct.* **22** 150–8

[27] Rizzo R, Musolino A, Bucchi F, Forte P and Frendo F 2014 Magnetic FEM design and experimental validation of an innovative fail-safe magnetorheological clutch excited by permanent magnets *IEEE Trans. Energy Convers.* **29** 628–40

[28] Rizzo R, Musolino A, Bucchi F, Forte P and Frendo F 2015 A multi-gap magnetorheological clutch with permanent magnet *Smart Mater. Struct.* **24** 075012

[29] Rizzo R 2016 An innovative multi-gap clutch based on magneto-rheological fluids and electrodynamic effects: magnetic design and experimental characterization *Smart Mater. Struct.* **26** 015007

[30] Wang D, Zi B, Zeng Y, Qian S and Qian J 2017 Simulation and experiment on transient temperature field of a magnetorheological clutch for vehicle application *Smart Mater. Struct.* **26** 095020

[31] Chen D, Xu J, Pan J, Guo X and Sun W 2012 Research and prospect of automobile magneto-rheological fluid dual clutch transmission *Proc. 2nd Int. Conf. Electronic & Mechanical Engineering and Information Technology Shenyang, China* pp 98–102

[32] Dai S, Du C and Yu G 2013 Design, testing and analysis of a novel composite magnetorheological fluid clutch *J. Intell. Mater. Syst. Struct.* **24** 1675–82

[33] Kim W H, Park J H, Kim G-W, Shin C S and Choi S-B 2017 Durability investigation on torque control of a magneto-rheological brake: experimental work *Smart Mater. Struct.* **26** 037001

[34] Nguyen Q and Choi S 2012 Optimal design of a novel hybrid MR brake for motorcycles considering axial and radial magnetic flux *Smart Mater. Struct.* **21** 055003

[35] Zubieta M, Eceolaza S, Elejabarrieta M and Bou-Ali M 2009 Magnetorheological fluids: characterization and modeling of magnetization *Smart Mater. Struct.* **18** 095019

[36] Nguyen Q and Choi S 2010 Optimal design of an automotive magnetorheological brake considering geometric dimensions and zero-field friction heat *Smart Mater. Struct.* **19** 115024

[37] Fu H Y, Zu Zhi T and Nan W N 2010 Numerical calculation of torque transmission and magnetic circuit finite element analysis of a magnetorheological clutch *2010 Int. Conf. Computing, Control and Industrial Engineering* vol 1 (IEEE) pp 403–7

[38] Lee D-Y and Wereley N M 1999 Quasi-steady Herschel-Bulkley analysis of electroand magneto-rheological flow mode dampers *J. Intell. Mater. Syst. Struct.* **10** 761–9